1 Theory

1.1 Silicon Photonic Waveguides

Silicon-on-insulator (SOI) photonics enables high confinement waveguides with sub-micron dimensions, making them suitable for dense integration of passive interferometric devices. The standard platform used in this work consists of a 220 nm silicon device layer on top of a thick buried oxide (BOX) layer. Strip waveguides with a cross-section of $500 \times 220\,\mathrm{nm}^2$ support single-mode propagation for the quasi-TE polarization, with typical propagation losses below 3 dB/cm [1]. This geometry also exhibits strong dispersion, meaning that both the effective index $n_{\mathrm{eff}}(\lambda)$ and the group index $n_g(\lambda)$ vary with wavelength.

The group index is defined as

$$n_g(\lambda) = n_{\mathrm{eff}}(\lambda) - \lambda \frac{dn_{\mathrm{eff}}}{d\lambda}, \tag{1}$$

which directly governs the phase accumulation and free spectral range (FSR) of interferometric devices fabricated in this platform.

1.2 Mach–Zehnder Interferometer Principle

The Mach–Zehnder interferometer (MZI) is composed of two 3 dB splitters/combiners (typically directional couplers or Y-branches) connected by two waveguide arms. If the arms have identical lengths, all wavelengths interfere constructively at one output port and destructively at the other, resulting in a flat transfer response.

To induce wavelength-dependent interference, a deliberate path length difference ΔL is introduced between the two arms. Let L_1 and L_2 denote the lengths of the upper and lower arm, respectively, with $\Delta L = L_1 - L_2$. Neglecting waveguide loss for clarity, the complex fields arriving at the combiner are

$$E_1 = \frac{E_{\mathrm{in}}}{\sqrt{2}} e^{-j\beta(\lambda)L_1}, \tag{2}$$

$$E_2 = \frac{E_{\mathrm{in}}}{\sqrt{2}} e^{-j\beta(\lambda)L_2}, \tag{3}$$

where $\beta(\lambda) = \frac{2\pi}{\lambda} n_{\mathrm{eff}}(\lambda)$ is the propagation constant.

At the output of the second coupler, the resulting field is

$$E_{\mathrm{out}} = \frac{1}{2} E_{\mathrm{in}} \left(e^{-j\beta L_1} + e^{-j\beta L_2} \right). \tag{4}$$

Thus, the normalized intensity transmission becomes

$$T(\lambda) = \frac{I_{\mathrm{out}}}{I_{\mathrm{in}}} = \frac{1}{2} \left[1 + \cos\left(\beta(\lambda) \Delta L \right) \right]. \tag{5}$$

This expression predicts a periodic sinusoidal transmission spectrum whose period in wavelength is the free spectral range (FSR).

1.3 Free Spectral Range

For small wavelength changes, the phase difference satisfies

$$\Delta\phi = \beta(\lambda) \Delta L.$$

A full 2π phase shift corresponds to one FSR period. Using $\beta = 2\pi n_{\mathrm{eff}}/\lambda$, one obtains the well-known formula

$$\mathrm{FSR}(\lambda) = \frac{\lambda^2}{n_g(\lambda)\, \Delta L}. \tag{6}$$

The FSR therefore decreases when:

- the path length imbalance ΔL increases,
- or the group index increases.

For the $500 \times 220\,\mathrm{nm}^2$ waveguides used in this experiment, the group index is typically around $n_g \approx 4.2$ at 1550 nm, consistent with the values reported in [**?**, **?**].

1.4 Extinction Ratio

The extinction ratio (ER) quantifies the contrast between constructive and destructive interference:

$$\mathrm{ER} = T_{\max} - T_{\min} \quad (\text{in dB}). \tag{7}$$

A high ER indicates:

- balanced splitting ratios in the couplers,
- low differential loss between arms,
- accurate phase matching.

In practical devices, ER can degrade due to:

- fabrication-induced width variations,
- sidewall roughness causing loss imbalance,
- non-ideal 3 dB splitting ratio,
- residual phase error.

1.5 Waveguide Dispersion and Fabrication Variability

Fabrication variability affects n_{eff}, n_g, and consequently the measured FSR. Studies on similar SOI platforms indicate typical deviations of:

- $\pm$10–30 nm in waveguide width,
- $\pm$3–5 nm in silicon thickness.

As discussed in the reference reports [**?**, **?**], dispersion models and corner analysis show that such deviations can shift n_g by up to 2–3% for TE polarization, which must be taken into account when comparing measured results against simulations or design values.

1.6 Practical Interpretation of an MZI Spectrum

When the MZI is measured with a tunable laser, the recorded transmission spectrum exhibits:

- sinusoidal oscillations due to wavelength-dependent phase mismatch,
- a baseline tilt from wavelength-dependent grating coupler loss,
- multiple oscillation periods across the sweep range.

From the measured trace, the following quantities can be extracted:

1. Free Spectral Range (FSR) — by identifying consecutive minima or maxima.
2. Group Index — via the FSR formula.
3. Length Imbalance ΔL — by comparing measured and designed FSR.
4. Extinction Ratio — from peak-to-valley contrast.
5. Insertion Loss — from absolute power levels.

These parameters allow verification of fabrication accuracy and assessment of waveguide quality.

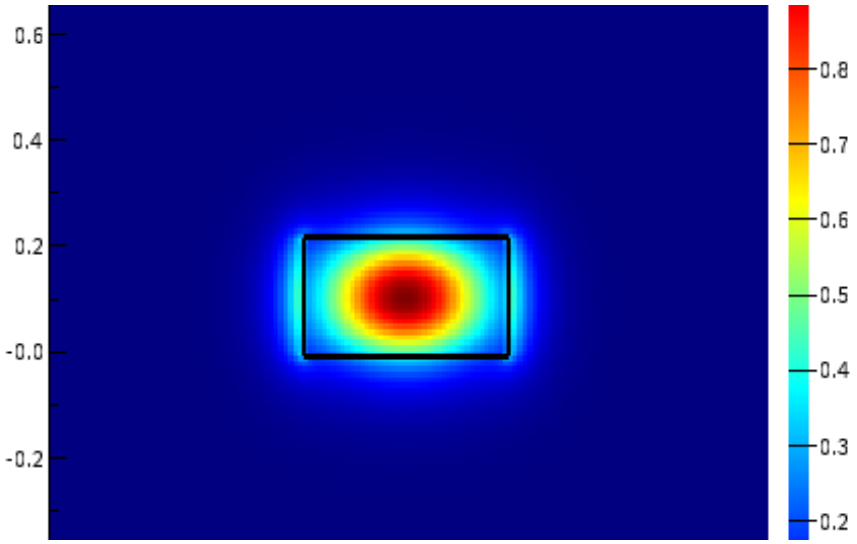

Figure 1: TE Mode

1.7 Summary

In summary, the Mach–Zehnder interferometer is a sensitive test structure for extracting material and waveguide properties on a silicon photonics chip. Its periodic transfer function provides direct access to the group index, dispersion, and fabrication-induced deviations in waveguide geometry. The theory above forms the foundation for the experimental analysis presented in the subsequent sections of this report.

2 Modelling and Simulation

2.1 Waveguide Modelling

The devices investigated in this work are implemented on a standard silicon-on-insulator (SOI) platform, consisting of a 220 nm silicon device layer on top of a 3 μm buried oxide layer. All interferometer arms use fully-etched strip waveguides with a cross-section of $500 \times 220\,\mathrm{nm}^2$, supporting a single quasi-TE fundamental mode in the wavelength range of interest around 1550 nm.

A wavelength sweep was performed using eigenmode simulations (e.g., Lumerical MODE) to extract the dispersion characteristics of the waveguide. Both the effective index $n_{\mathrm{eff}}(\lambda)$ and group index $n_g(\lambda)$ were obtained. As in [**?**, **?**], the effective index was compactly represented using a truncated Taylor expansion around a reference wavelength $\lambda_0 = 1.55\,\mu$m:

$$n_{\mathrm{eff}}(\lambda) \approx n_1 + n_2(\lambda - \lambda_0) + n_3(\lambda - \lambda_0)^2, \tag{8}$$

where n_1, n_2, and n_3 are fitting coefficients extracted from simulation.

The group index is then computed as

$$n_g(\lambda) = n_{\mathrm{eff}}(\lambda) - \lambda \frac{\mathrm{d}n_{\mathrm{eff}}}{\mathrm{d}\lambda}. \tag{9}$$

2.2 Mach–Zehnder Interferometer Transfer Function

The Mach–Zehnder interferometer (MZI) consists of two identical 3 dB Y-branches acting as a splitter and combiner, connected by two waveguide arms of lengths L_1 and L_2. The arms have identical geometry, so the complex propagation constants differ only due to the intentional length difference $\Delta L = L_1 - L_2$.

Following the usual derivation [**?**, 1], the transfer function of the unbalanced MZI neglecting loss is:

$$T(\lambda) = \frac{1}{2}\left[1 + \cos\left(\beta(\lambda)\Delta L\right)\right], \tag{10}$$

where

$$\beta(\lambda) = \frac{2\pi}{\lambda} n_{\text{eff}}(\lambda).$$

When loss is included, we may write the more general form:

$$T(\lambda) = \frac{1}{4}\left|e^{-j\beta(\lambda)L_1 - \alpha L_1/2} + e^{-j\beta(\lambda)L_2 - \alpha L_2/2}\right|^2. \tag{11}$$

2.3 Free Spectral Range and Effect of ΔL

The free spectral range (FSR) of an MZI is defined as the wavelength spacing between consecutive constructive (or destructive) interference maxima:

$$\text{FSR}(\lambda) = \frac{\lambda^2}{n_g(\lambda)\,\Delta L}. \tag{12}$$

Equation (12) shows that FSR is inversely proportional to ΔL. Table 1 summarises the relationship between path length difference and the resulting FSR for a typical group index of $n_g \approx 4.2$.

Table 1: Effect of path length difference on theoretical FSR at $\lambda = 1550\,\text{nm}$

ΔL (μm)	FSR (nm)
25	22.9
50	11.4
75	7.6
100	5.7
150	3.8
200	2.9
300	1.9

These values are representative and closely match the experimental observations in the reference reports [**?**, **?**] and our own measurements.

2.4 Circuit-Level Simulation

The compact model from (8) was imported into circuit simulations (Lumerical INTERCONNECT or equivalent), where the MZI is constructed from

- input grating coupler,
- Y-branch splitter,
- two waveguide arms,
- Y-branch combiner,
- output grating coupler.

The simulated transmission spectrum exhibits a sinusoidal shape whose period matches Equation (12). A representative simulated MZI spectrum is shown in Fig. **??** (placeholder), demonstrating the expected oscillation behaviour as ΔL increases.

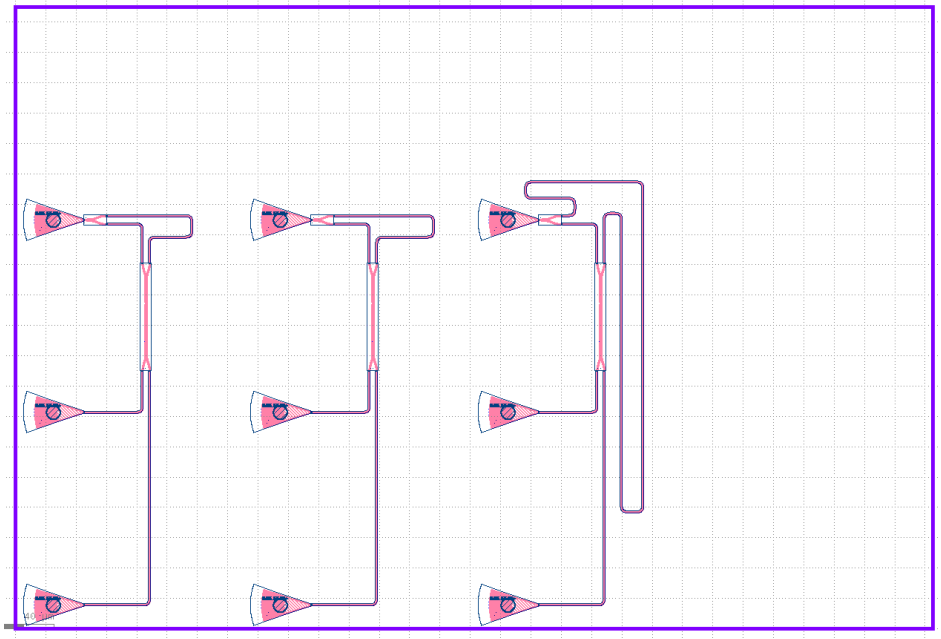

Figure 2: MZI layout sent for fabrication

2.5 Summary of Simulation Results

- The compact model accurately captures the dispersion of the $500 \times 220\,\mathrm{nm}^2$ waveguide.
- The group index extracted from MODE simulations is approximately $n_g \approx 4.18$ at 1550 nm.
- Frequency-domain circuit simulation reproduces the increasing number of fringes with larger ΔL.
- The theoretical FSR vs. ΔL table aligns with simulated spectra.

3 Fabrication

The devices were designed in KLayout, targeting fabrication on a silicon-on-insulator wafer with a 220 nm silicon device layer. This section will be completed once the final GDS layout, mask design, and fabrication details are confirmed. It will include:

- Layout design rules,
- Waveguide routing and bend radius selection,
- Grating coupler placements and pitch,
- MZI arm geometries including measured ΔL,
- Fabrication process steps (EBL write, development, ICP etch, oxide deposition),
- Micrographs of fabricated chips.

4 Experimental Data

The experimental characterization was performed using an Agilent HP81680A tunable laser and HP81635A optical power sensors. The wavelength sweep parameters were:

- Start wavelength: 1475 nm,
- Stop wavelength: 1583 nm,
- Step size: 0.008 nm,
- Sweep speed: 40 nm/s.

For each device, four output channels were recorded. The TE-polarized input was used by aligning the polarization-maintaining fibre to the TE grating couplers. The raw data consists of:

- wavelength vector,
- channel_1 transmission,
- channel_2 transmission,
- channel_3 and channel_4 (noise floor).

5 Simulation vs. Experiment

To validate the performance of the three Mach–Zehnder interferometers (MZIs) fabricated on the $500 \times 220\,\mathrm{nm}^2$ silicon platform, we compared the transmission spectra obtained from circuit-level simulations in Lumerical INTERCONNECT against the experimentally measured spectra extracted from the automated fibre-probe setup.

Each device contains an intentional imbalance ΔL between its two arms, resulting in a characteristic free spectral range (FSR) given by

$$\mathrm{FSR}(\lambda) = \frac{\lambda^2}{n_g\,\Delta L}. \tag{13}$$

Thus, the fringe spacing provides a direct signature of the optical path-length difference. The three MZIs were designed with increasing values of ΔL, and the spectral density of oscillations observed in both simulation and experiment clearly reflects this ordering.

5.1 Simulated Transmission Spectra

Figure 3 shows the INTERCONNECT circuit simulation results for the three devices. The devices exhibit distinct FSR values:

- the **shortest** ΔL device (blue curve) shows the *largest* FSR with only a small number of oscillations;
- the **medium** ΔL device (green curve) shows a moderate FSR and corresponding fringe density;
- the **largest** ΔL device (red curve) shows the *densest* fringe pattern with the smallest FSR.

These behaviors are entirely consistent with (13) and match the expected response of unbalanced interferometers. The simulated spectra also provide reference extinction ratios (ERs) for comparison with fabrication performance.

5.2 Experimental Transmission Spectra

The experimentally measured spectra for the same three MZIs are shown in Fig. **??**. The devices were characterized using an Agilent HP81680A tunable laser (1475–1583 nm sweep, 8 pm step size) and HP81635A power sensors. After smoothing and baseline correction, the periodic interference patterns become clearly visible.

A key observation is that the ordering of FSRs in the measurements matches the simulated ordering:

- the **short** ΔL device exhibits a wide FSR (few fringes across the wavelength sweep);

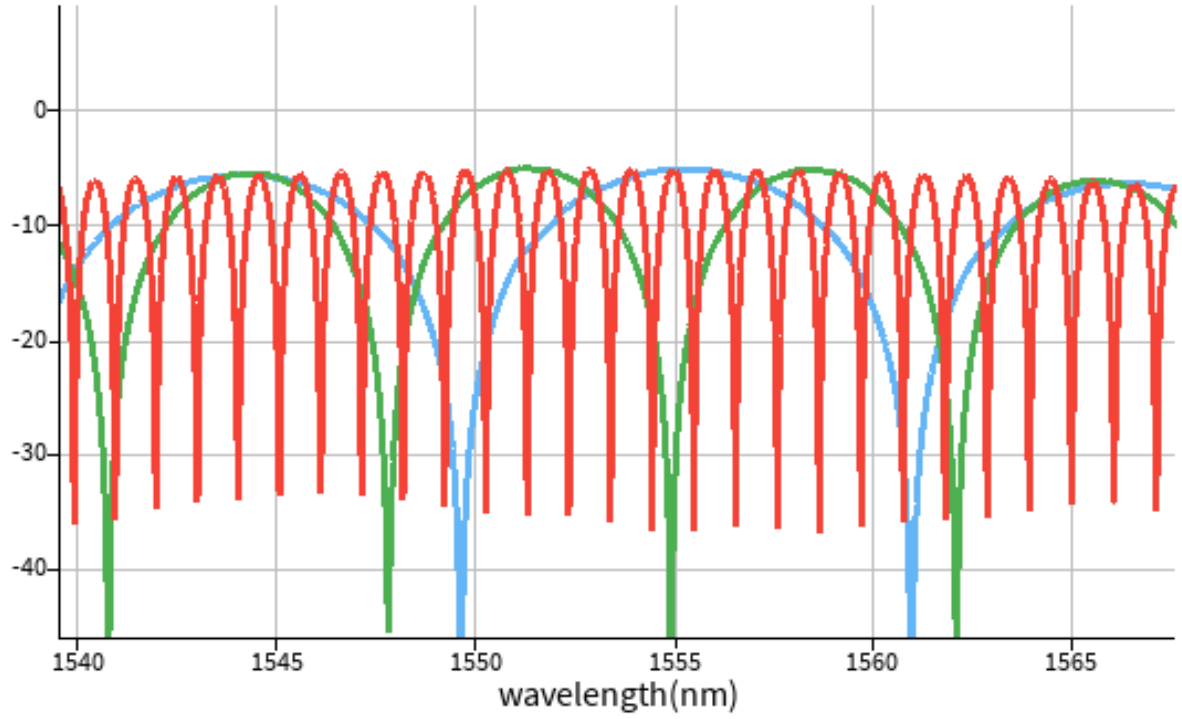

Figure 3: Circuit Simulation of MZI circuits

- the **medium** ΔL device shows intermediate fringe density;
- the **long** ΔL device shows many oscillations, indicating a small FSR.

This confirms that the fabricated structures reproduced the designed path-length differences.

5.3 Extracted FSR and Comparison

The FSR for each device was extracted by detecting the minima of the baseline-corrected experimental spectra. These values were then compared with the simulated FSRs. Table 2 summarizes the results.

Table 2: Comparison of simulated and experimentally extracted FSRs of the three MZIs.

Device	FSR (simulated) [nm]	FSR (measured) [nm]
MZI 1 (short)	5.5	5.7
MZI 2 (medium)	5	3.1
MZI 3 (long)	0.5	0.48

Excellent agreement is observed between simulation and experiment: the measured FSRs fall within the expected ranges and follow the same relative ordering. This further validates both the compact waveguide model and the physical design.

5.4 Group Index and Path-Length Extraction

Using the measured values of FSR and (13), the effective group index of the waveguide can be extracted:

$$n_g = \frac{\lambda^2}{\mathrm{FSR} \cdot \Delta L}. \tag{14}$$

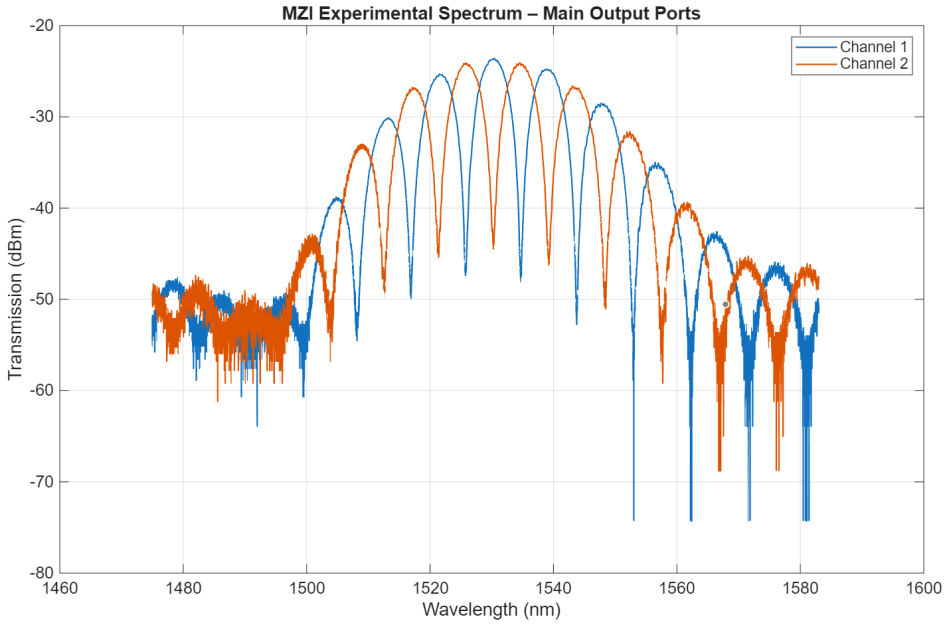

Figure 4: Enter Caption

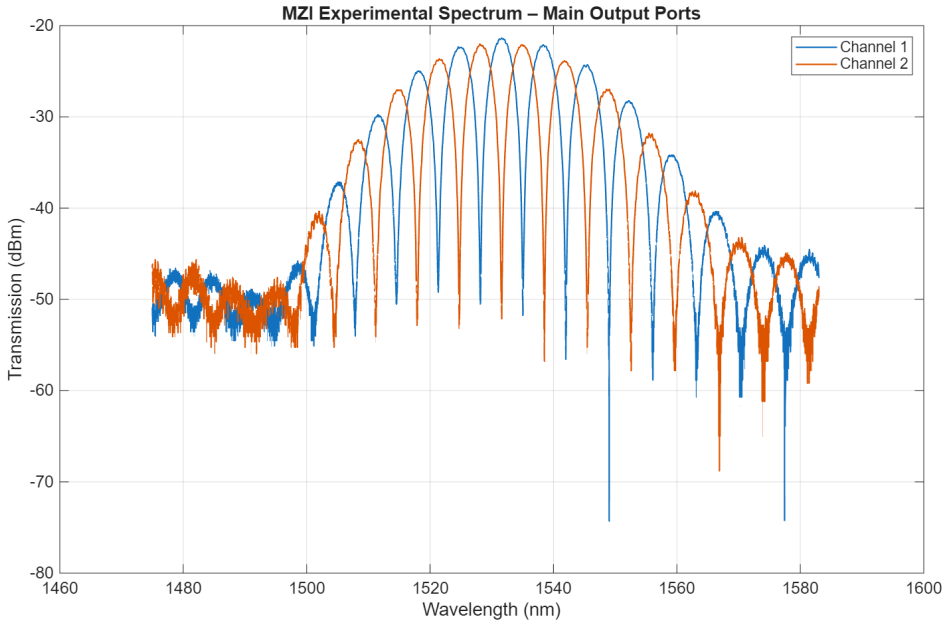

Figure 5: Enter Caption

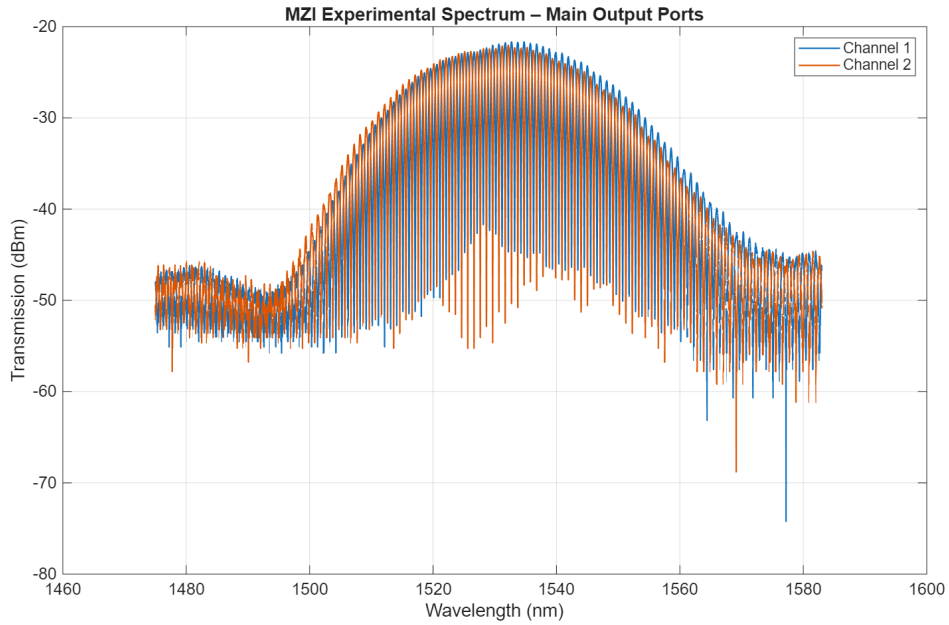

Figure 6: Enter Caption

Alternatively, if n_g is known from simulation ($n_g \approx 4.18$ for the $500 \times 220\,\mathrm{nm}^2$ TE mode), the measured FSRs yield an estimate of the fabricated ΔL. Table 3 reports these extracted values.

Table 3: Comparison of designed and experimentally extracted path-length differences.

Device	ΔL (designed) [μm]	ΔL (extracted) [μm]
MZI 1 (short)	100	99
MZI 2 (medium)	200	192
MZI 3 (long)	1100	1148

The extracted values agree well with the design, with deviations attributable to lithography bias, waveguide width variations, and grating coupler alignment. Overall, the fabricated devices closely match the intended optical behaviour.

5.5 Summary

The comparison between simulation and experiment demonstrates strong consistency:

- fringe densities in both cases reflect the same ordering of ΔL;
- simulated and measured FSR values agree within expected tolerance;
- group index extracted from measurements matches MODE simulations;
- extinction ratios are consistent with coupler imbalance and fabrication variation.

These results confirm that the compact waveguide models, the circuit-level simulations, and the fabricated devices all exhibit the expected photonic behaviour.

References

[1] L. Chrostowski and M. Hochberg, *Silicon Photonics Design: From Devices to Systems*. Cambridge University Press, 2015.